Application of synchrotron X-ray microtomography to investigate ductile fracture in Al alloys

Qian, L.
Department of Production Systems, Toyohashi University of Technology

Toda, Hiroyuki
Department of Production Systems, Toyohashi University of Technology

Uesugi, kentaro
Japan Synchrotron Radiation Research Institute

Kobayashi, T.
Department of Production Systems, Toyohashi University of Technology

他

出版情報：Applied physics letters. 87 (24), pp.241907-, 2005-12-01. American Institute of Physics
バージョン：
権利関係：

Application of synchrotron X-ray microtomography to investigate ductile fracture in Al alloys

L. Qian and H. Toda

Department of Production Systems, Toyohashi University of Technology, Toyohashi, 441-8580, Japan

K. Uesugi

Japan Synchrotron Radiation Research Institute, Sayo, Hyogo, 679-5198, Japan

T. Kobayashi, T. Ohgaki, and M. Kobayashi

Department of Production Systems, Toyohashi University of Technology, Toyohashi, 441-8580, Japan

The in-situ high-resolution synchrotron X-ray computed microtomography has been applied to visualize and quantify the ductile fracture process of a notched Al alloy specimen. The three-dimensional (3D) investigation reveals that voids are nucleated, grow and coalesce more easily near the notch front and in the central region of the sample. These voids are mainly associated to Si particles in the eutectic phase (EU). The 3D packing architecture of particles in the EU region, and the 3D morphology of α-phase are also visualized. The feasibility of this technique highlights the potential of its application in the field of micromechanics-based fracture.

Traditional methods such as optical and scanning electron microscopy have become the common tools for investigating crack growth behavior in materials. These methods provide important information on two-dimensional (2D) fracture, and fracture mechanisms concerned are accordingly proposed, thereby analysis models are established.[1-3] However, fracture in the interior differs from the surface even if the material is uniform. If a crack appears stagnant on the surface, it may have grown for a significant distance in the internal because of the difference in stress-strain states. For a practical material with a complicated microstructure, the fracture is even more complex from a 3D point of view. Thus, 3D investigation of fracture in a material is of great importance. For this purpose, some work has been attempted to understand the fracture features beneath the surface via serial sectioning of a sample.[4-6] However, this technique is laborious and destructive, obtainable information is limited and errors may arise due to sample preparation.

The X-ray computed microtomography provides information on the internal structural features of a material by the measurements of the attenuation of an X-ray passing through the sample at different incidence angles.[7,8] It has many applications in a variety of fields, such as for the identification of internal material inhomogeneities, assessment of internal defects and damage, and investigation of the microstructure-property relationships in various materials.[9-15] The X-ray microtomography is also expected to have a good perspective in fracture studies, however, a particularly high spatial resolution well suited for the investigation of crack and crack/microstructure interaction is much required.[16,17] Fortunately, the currently largest third-generation synchrotron radiation facility at the SPring-8 in Japan enables X-ray computed tomography with a high resolution down to less than 1 μm.[18,19] In this letter, an in-situ 3D visualization and quantification of ductile fracture process in a practical Al alloy characterized by initiation, growth and coalescence of voids are performed by this advanced technique. Hence, a better understanding of the micromechanims of ductile

fracture is anticipated.

A cast A356 Al alloy, which consists of a soft α phase and a eutectic phase, was selected. The tensile specimen with a parallel length of 12 mm and a square cross section of 0.56×0.56 mm^2 was prepared. In the middle of the parallel section, a notch with a width of 0.14 mm and a depth of 0.28 mm was machined using the electric discharging machining.

High-resolution X-ray tomography was carried out at the X-ray imaging beamline BL47XU of the third-generation synchrotron radiation facility in Japan. Monochromatic X-ray beams with a beam energy of 20keV coming from a double crystal monochromator were applied. The in-situ tomography was performed during tensile loading. In-situ tensile test was conducted using a test rig specially designed for the X-ray tomography at the SPring-8.[18,19] The controller of the test rig has a load resolution of 0.1 N and displacement resolution of 0.8 μm, and loading rate can be well controlled down to 0.1μm/sec, enabling well-controllable quasi-static tests using a miniaturized specimen. A PC tube was set on a rotation stage, and used as a frame for transferring the load between the upper and lower loading grips. This tube was carefully polished, thus giving uniform and negligible X-ray absorption. The test sample set in the test rig was placed 49 m away from the X-ray source. A cooled 4000×2624 element CCD camera (binning mode) was put at 50 mm behind the sample to record the projections of all scans. The choice of such a sample/camera distance was to obtain some phase contrast in the reconstructed images.[9] The tensile load was applied by successively increasing displacement. Three tomography scans were made in the same sample, one prior to loading and the other two at different loading states. Each scan of the sample consisting of recording 1500 slice radiographs was performed during a 180^0 rotation along a vertical axis. In the case of loading states, the scans were made during holding the sample at a fixed displacement. The size of an isotropic voxel in the subsequently reconstructed images was $(0.474\mu m)^3$.

The images were reconstructed using the filtered back-projection algorithm. The reconstructed slice images were then rendered using a visualization software. Furthermore, segmentation was performed to quantitatively analyze the generated voids and their growth in the sample with increasing load. An in-house soft code was used to calculate the size, number and distribution of the voids.

The reconstructed 3D rendering of the unloaded microstructure of the present material is shown in Fig. 1. The network structure with Si particles belongs to Al-Si eutectic phase while the large cell-shaped regions surrounded by the EU phase belong to primary α phase dendrite cells. The 3D packing architecture of Si particles is clearly visualized. Fig. 2 shows the slice images of the same cross section at the two loading states. The cross section lies parallel to the loading direction near the midplane of the specimen. At a load of 51.6 N, voids are nucleated in front of the notch (Fig. 2(a)). With an increase in load (55.0 N, Fig. 2(b)), previously generated voids increase in size, and some adjacent ones coalesce with each other. Some newly initiated voids are also visible. Other slices parallel to the one in Fig. 2 show that the number, size and shape of the voids differ so much from slice to slice. At some slices, voids are connected covering a length of more than 60 μm while at some other slices voids are still separated without obvious coalescence. At the slices near the specimen side surfaces, only a few small voids are observable. In addition, the voids occur mainly within the eutectic regions and are closely related to the eutectic particles.

The 3D images of the same extracted volume at the two loading states are presented in Fig. 3(a) and (b), respectively. On the whole, high density of voids is mainly concentrated near the notch front. Comparison of Fig. 3(a) and (b) indicates that increasing load causes an increase in the number and size of voids. The 3D coalescence of voids is easily visible. The morphologies of various voids within any arbitrary region of interest can also conveniently be examined from different view angles. From the magnified views (Fig. 3(c) and (d)), it can be

seen that the voids at positions 1 and 2 are protruded out but partly embedded inside the solid material. They lie exactly at the Si particles, further indicating that the void initiation is caused by the damage at particles. When increasing load, the above two voids are expanded and elongated, and void 2 tends to reach the cloud of voids in its front. Moreover, one can see new voids generated at position 3 in Fig. 3(d), which are not visible in Fig. 3(c).

To quantify the 3D void distribution, voids only are preserved while other material constituents in the extracted volume (0.04 mm^3) are removed. The shape (i.e. sphericity) and the volume of each void are obtained by calculating the number of voxels of the void. Most of the voids are found to be smaller than 200 μm^3 while there indeed exist a small number of larger voids (~ 1000 μm^3). The voids do not take spherical but prolate or oval shape, indicating non-isotropic growth of the voids. This is reasonable since the voids tend to initiate in the EU phase and grow preferably within the narrow wall of the network region. The number of voids per 0.001mm^3 along x or y directions are calculated. The spatial location of a void is determined by the center of the object voxels corresponding to the void. The distributions of the generated voids are plotted in Fig. 4(a) and (b), as a function of distance from the notch front along y direction. Almost all the voids are located within a region of ~150 μm from the notch front. Both the number and volume show an obviously decreasing tendency when departing from the notch. These values become even larger at loading stage 2. The number and volume of voids as a function of distance from one side surface to another of the specimen along x direction are shown in Fig. 4(c) and (d), respectively. There exist only a few tiny voids on both sides while more and larger voids are generated in the central region. Increasing load leads to a rise in both the number and size of voids.

The above visualization results are consistent with the known fracture mechanics theory. In a notched specimen, stress and strain are concentrated near the notch front, and decrease with the distance. As is known, voids are initiated from damaged particles, which is controlled

by the local stress.[20,21] This explains why the number and size of voids show a decreasing tendency (Fig. 4(a) and (b)). Besides, both the number and size increase from the side surfaces to the central region (Fig. 4(c) and (d)). This is due to the lower constraint near the side surface compared to the midsection, and thus the void initiation is retarded and void growth is decelerated.[22] This result strongly suggests that the measurement at the side surface of a sample by means of the traditional 2D observations might not represent the bulk behavior. Additionally, one may note that the maximums of both number and size are not exactly located at the notch front in Fig. 4(a) and (b). And there exist several peaks on each data set in Fig. 4(c) and (d), showing wave-like change tendency. The mean distance between the peaks of the "wave", ~100μm, is of the same order of the size of α-phase, indicating that the non-monotonic change in size and number of voids is due to the non-uniform distribution of particles that are embedded in the EU region.

In the present work, the high-resolution synchrotron X-ray tomography has been demonstrated to be a feasible way to visualize and quantify the ductile fracture, and provide much more information than traditional methods. The feasibility of this technique shows the potential of its application in the field of micromechanics-based fracture, which enables not only to well understand the micromechanisms of fracture phenomena and examine the proposed micromechanical models but to provide 3D microstructural information as input data for image-based numerical simulations of fracture behaviors in various materials.

The synchrotron radiation experiments were performed at the SPring-8 with the approval of JASRI through proposal number 2004B0457-NI-np. The authors also acknowledge the Grant-in-aid for Scientific Research from JSPS through subject Nos. 17360340 and 16-04370.

References

[1] C. Motz and R. Pippan, Acta Mater. 50, 2013 (2002).

[2] H. Andersson and C. Persson, Int. J. Fatigue 26, 211 (2004).

[3] L. Qian, H. Toda, S. Morita, T. Kobayashi, and Z-G Wang, Mater. Trans. 46, 34 (2005).

[4] J. Alkemper and P. W. Voorhees, J. Microsc. 201, 388 (2001).

[5] M. V. Kral and G. Spanos, Scripta Mater. 36, 875 (1997).

[6] C. M. Dinnis, A. K. Dahle, and J. A. Taylor, Mater. Sci. Eng., A 392, 440 (2005).

[7] B. P. Flannery, H. W. Deckman, W. G. Roberge, and K. L. D'Amico, Science 237, 1439 (1987).

[8] Y. Nagata, H. Yamaji, K. Hayashi, K. Kawashima, K. Hyodo, H. Kawata, and M. Ando, Rev. Sci. Instrum. 63, 615 (1992).

[9] P. Cloetens, M. Pateyron-Salome, J. -Y. Buffiere, G. Peix, J. Baruchel, and F. Peyrin, J. Appl. Phys. 81, 5878 (1997).

[10] H. Bart-Smith, A. F. Bastawros, D. R. Mumm, A. G. Evans, D. J. Sypeck, and H. N. G. Wadley, Acta Mater. 46, 3583 (1998).

[11]T. Ohgaki, H. Toda, I. Sinclair, J. -Y. Buffiere, W. Ludwig, T. Kobayashi, M. Niinomi, and T. Akahori, Mater. Sci. Eng. A 406, 261 (2005).

[12] R. K. Everett, K. E. Simmonds, and A. B. Geltmacher, Scripta Mater. 44, 165 (2001).

[13] P. J. Schilling, B. R. Karedla, A. K. Tatiparthi, M. A. Verges, and P. D. Herrington, Comp. Sci. Tech. 65, 2071 (2005).

[14] A. Kulkarni, H. Herman, F. DeCarlo, and R. Subramanian, Metall. Mater. Trans. A 35, 1945 (2004).

[15] S. R. Stock, Int. Mater. Rev. 44, 141 (1999).

[16] H. Toda, I. Sinclair, J.-Y. Buffière, E. Maire, T. Connolley, M. Joyce, K.H. Khor, and P. Gregson, Phil. Mag. 83, 2429 (2003).

[17] H. Toda, I. Sinclair, J. -Y. Buffiere, E. Maire, K. H. Khor, P. Gregson, and T. Kobayashi Acta Mater. 52, 1305 (2004).

[18] H. Toda, T. Ohgaki, K. Uesugi, K. Makii, Y. Aruga, T. Akahori, M. Niinomi, and T. Kobayashi, Key Eng. Mater. 1189, 297 (2005).

[19] T. Ohgaki, H. Toda, M. Kobayashi, K. Uesugi, M. Niinomi, T. Akahori, T. Kobayashi, K. Makii, and Y. Aruga, Philos. Mag., in review.

[20] A. S. Argon, J. Im, and T. Needleman, Metall. Trans. 6, 815 (1975).

[21] F. M. Beremin, Metall. Trans. 12, 723 (1981).

[22] *Fracture Mechanics: fundamentals and applications*, edited by T. L. Anderson (CRC press, USA, 1995), 281.

Figure captions

FIG. 1. Reconstructed 3D microstructure based on volume rendering. In the front half of the image, aluminum is removed to reveal the 3D shape and distribution of Si particles.

FIG. 2. Slice images of the same cross section near the middle of the specimen. They were captured under two applied loads of (a) 51.6 N and (b) 55.0 N.

FIG. 3. 3D rendering of the same extracted volume under loads of (a) 51.6 N and (b) 55.0 N. In each front half image, aluminum and particles are removed to highlight the voids. (c) and (d) are magnified views of the notch-front region in (a) and (b), respectively.

FIG. 4. Distributions of the number and volume of voids along mode I crack growth direction ((a) and (b)) and along notch front line ((c) and (d)) at the two applied loads.

FIG. 1

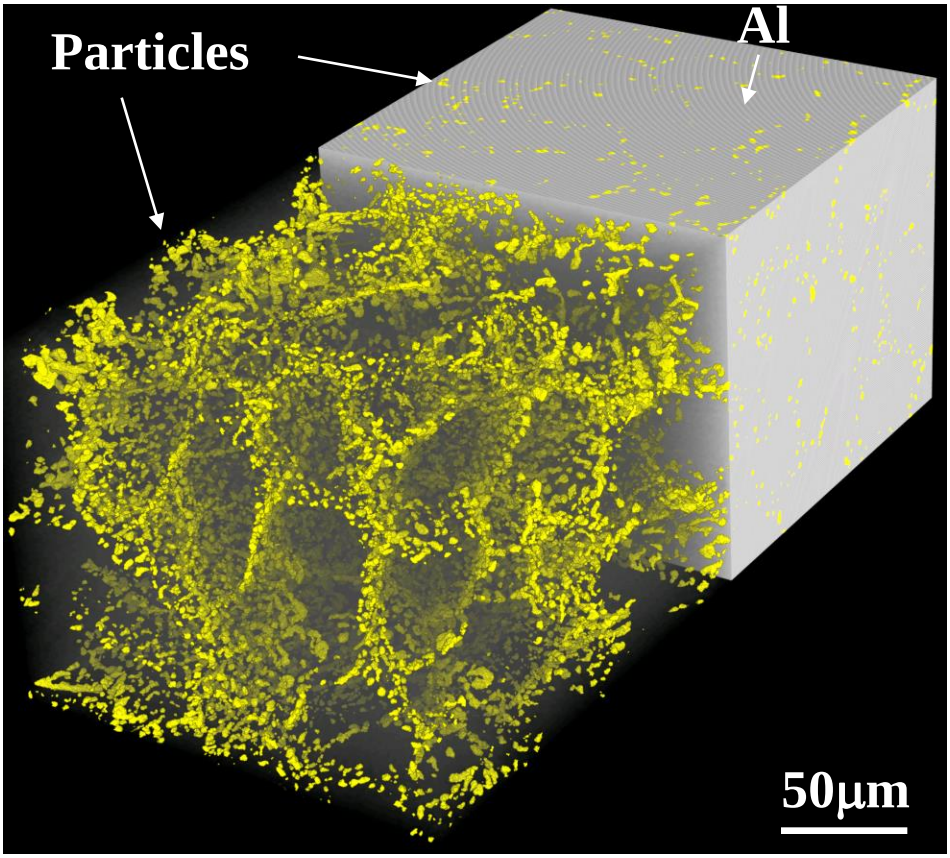

FIG. 2

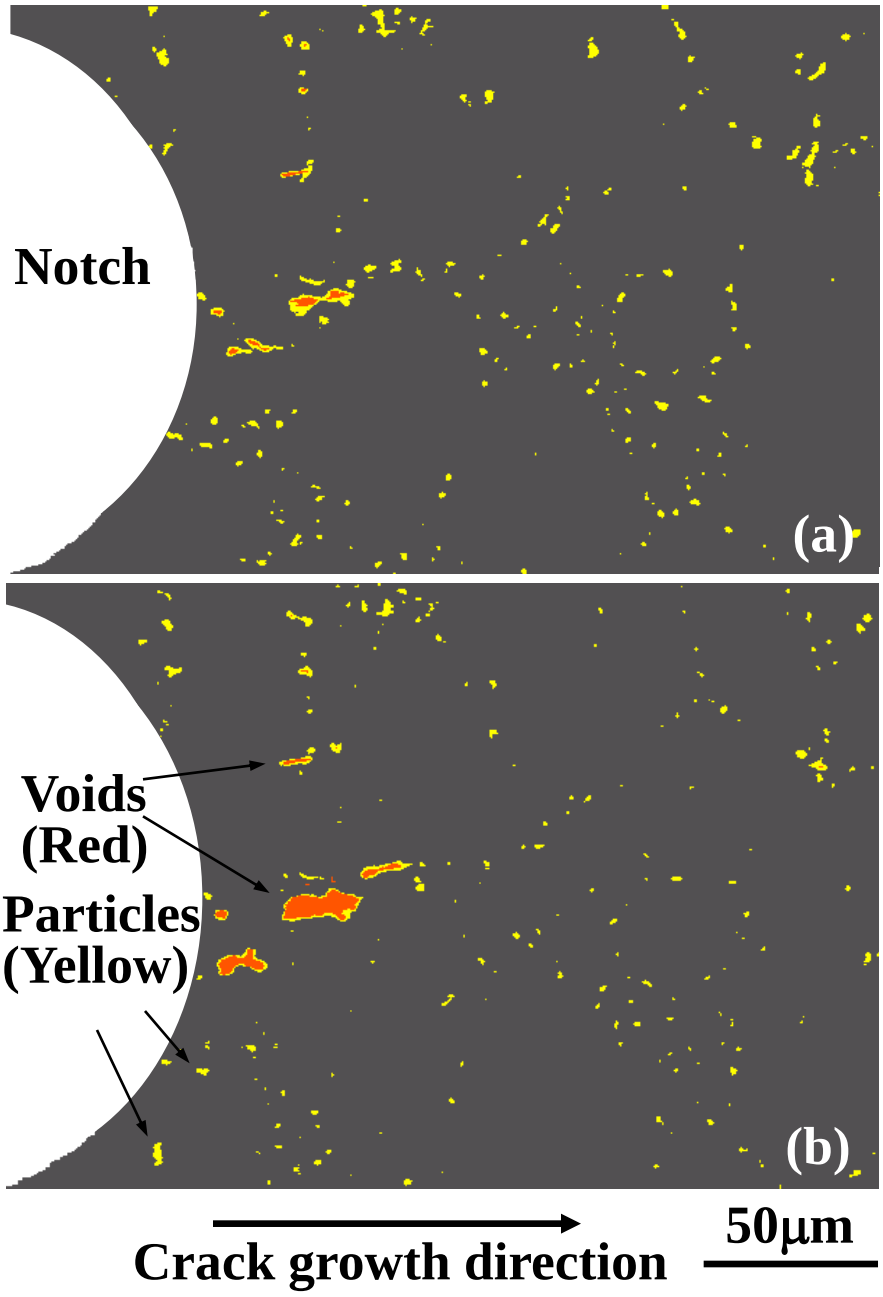
Notch
(a)
Voids
(Red)
Particles
(Yellow)
(b)
Crack growth direction
50μm

FIG. 3

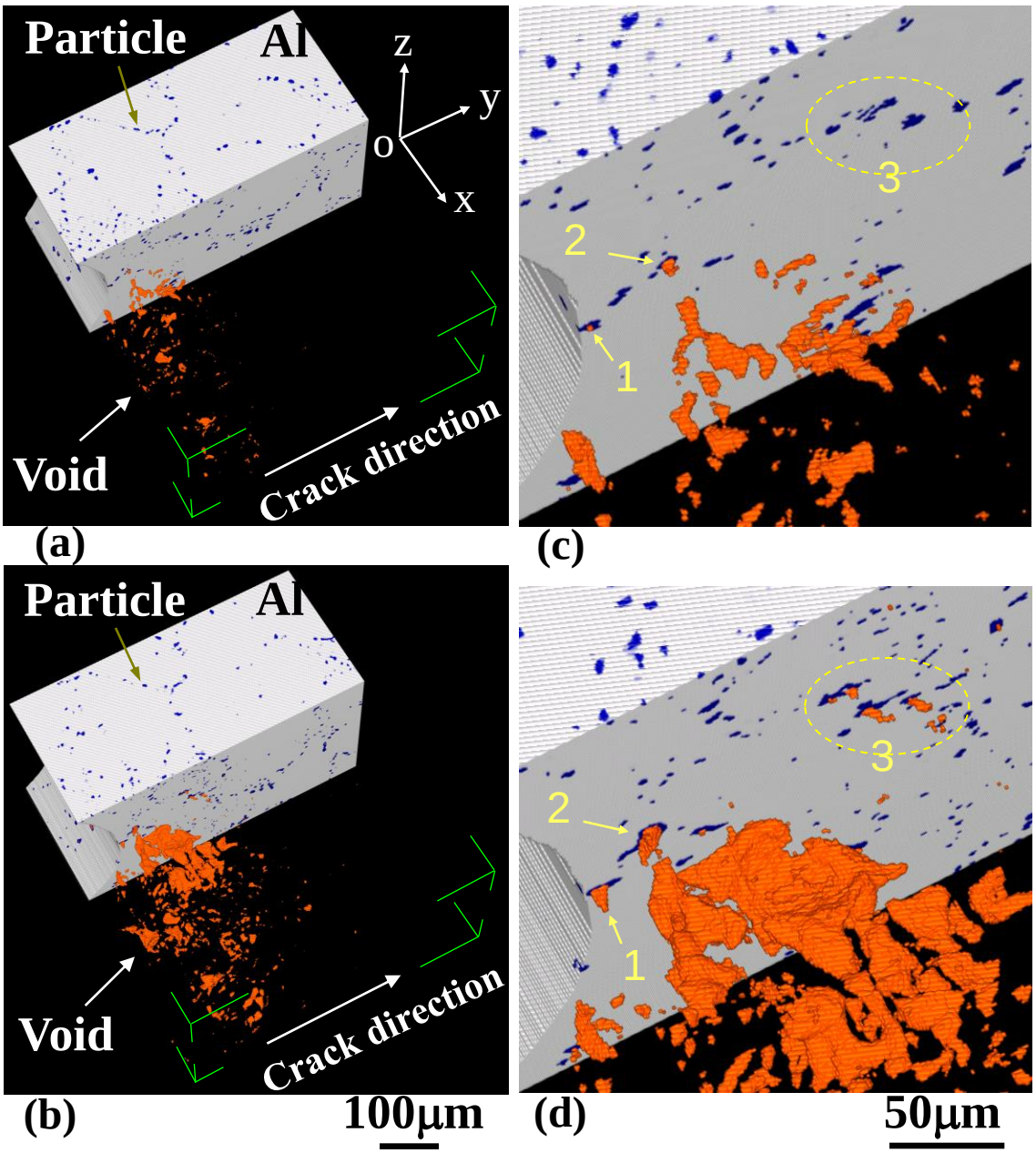
Particle
Al
z
y
o
x
Void
Crack direction
(a)
(c)
Particle
Al
Void
Crack direction
(b)
100μm
1
2
3
(d)
50μm

FIG. 4

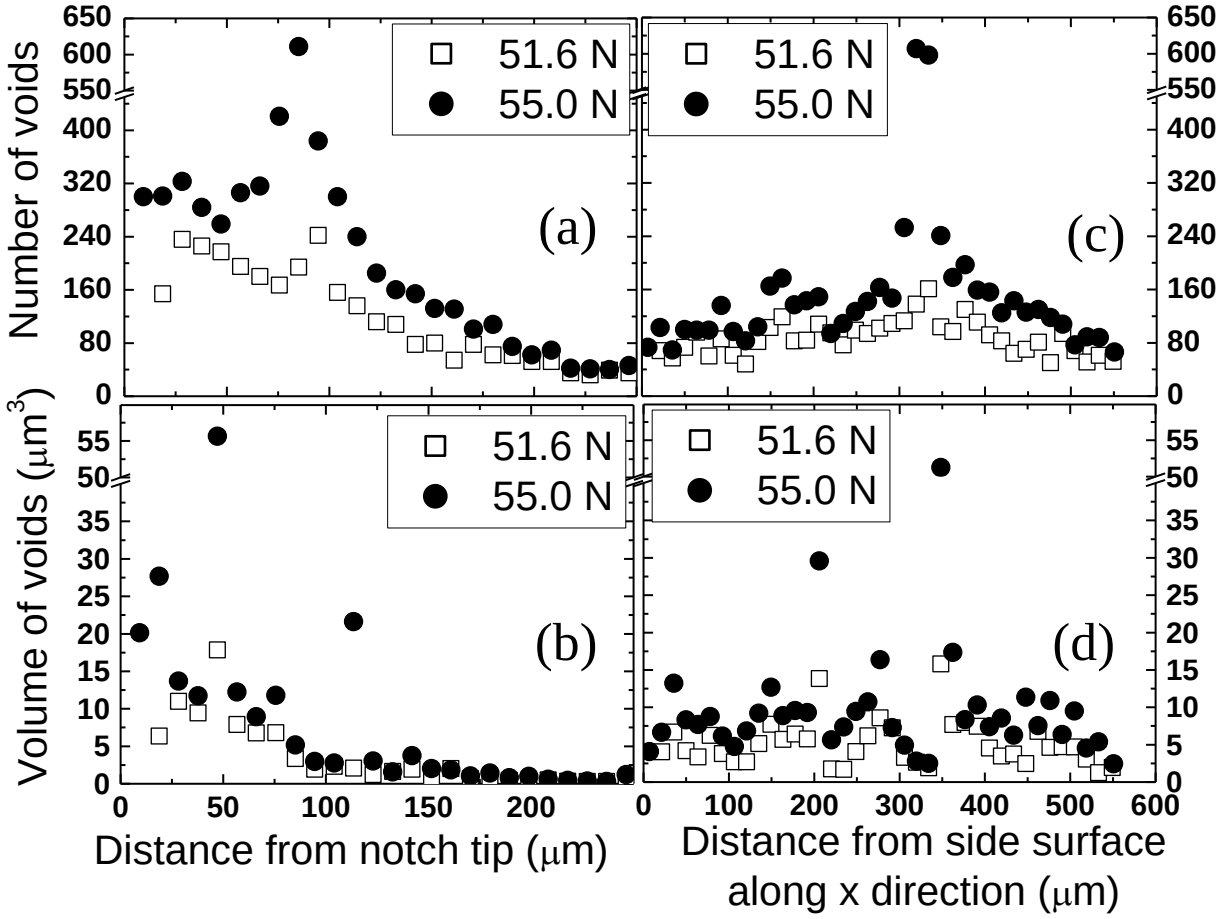
Number of voids
Volume of voids (μm³)
51.6 N
55.0 N
(a)
(b)
(c)
(d)
Distance from notch tip (μm)
Distance from side surface along x direction (μm)

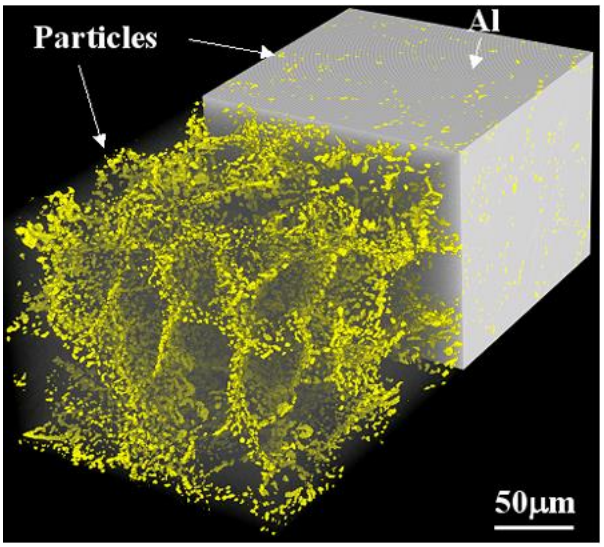
Particles
Al
50μm

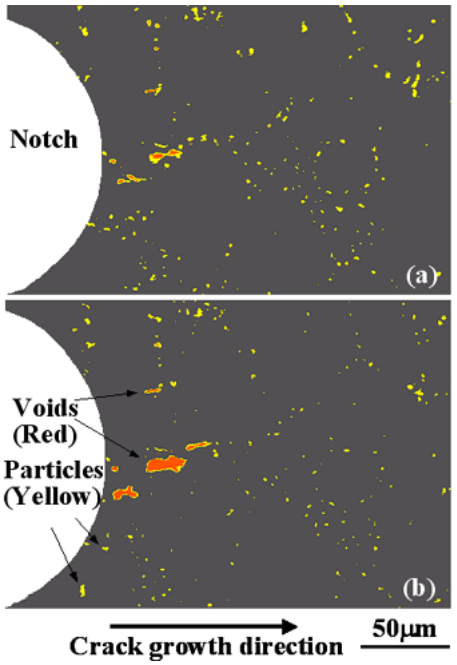
Notch
(a)
Voids
(Red)
Particles
(Yellow)
(b)
Crack growth direction
50μm

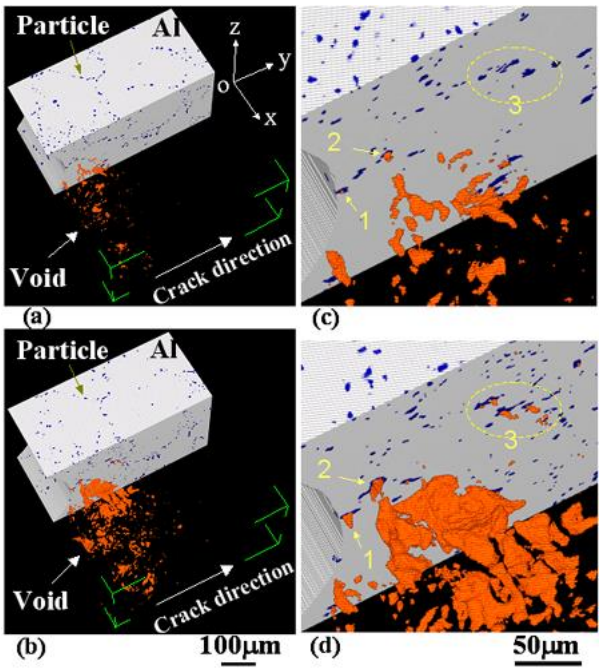
Particle
Al
z
y
x
o
Void
Crack direction
(a)
(c)
1
2
3
Particle
Al
Void
Crack direction
(b)
100μm
(d)
50μm

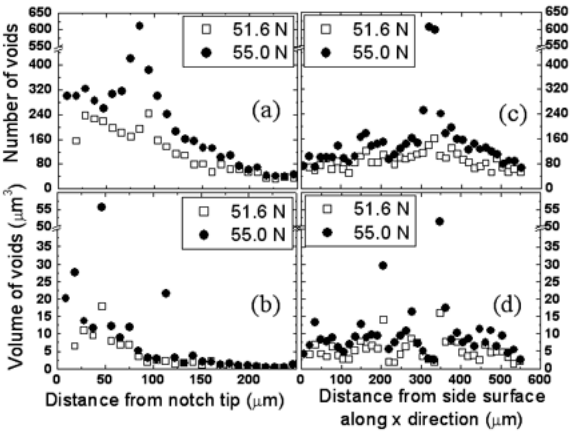
Number of voids
Volume of voids (μm³)
51.6 N
55.0 N
(a)
(b)
(c)
(d)
Distance from notch tip (μm)
Distance from side surface
along x direction (μm)